Supplementary information for

"Estimated regional CO_2 flux and uncertainty based on an ensemble of atmospheric CO_2 inversions"

Naveen Chandra[1], Prabir K. Patra[1,2,3], Yousuke Niwa[4], Akihiko Ito[4], Yosuke Iida[5], Daisuke Goto[6], Shinji Morimoto[3], Masayuki Kondo[7], Masayuki Takigawa[1], Tomohiro Hajima[1], Michio Watanabe[1]

[1]Research Institute for Global Change, JAMSTEC, 3173-25 Showa-machi, Kanazawa, Yokohama, 236-0001, Japan

[2]Center for Environmental Remote Sensing, Chiba University, Chiba, 263-8522, Japan

[3]Graduate School of Science, Tohoku University, 6-3 Aoba, Aramaki, Aoba-ku, Sendai 980-8578, Japan

[4]Earth System Division, National Institute for Environmental Studies, Tsukuba 305-8506, Japan

[5]Atmosphere and Ocean Department, Japan Meteorological Agency, Tokyo 105-8431, Japan

[6]National Institute of Polar Research, 10-3 Midori-cho, Tachikawa, Tokyo, 190-8518, Japan

[7]Institute for Space-Earth Environmental Research, Nagoya University, Nagoya, Aichi 464-8601 Japan

Correspondence to: Naveen Chandra (naveennegi@jamstec.go.jp) and Prabir K. Patra (prabir@jamstec.go.jp)

Table S1. A comprehensive list of CO_2 observations from 50 sites for optimizing fluxes, taken from GML/NOAA - Global Monitoring Laboratory/National Oceanic and Atmospheric Administration (38 sites), CSIRO - Commonwealth Scientific and Industrial Research Organisation (4 sites), LSCE/IPSL - Laboratoire des sciences du climat et de l'environnement/Institut Pierre Simon Laplace (1 site), SIO-CO2 – Scripps Institution of Oceanography (2 sites), SAWS – South African Weather Services (1 site), ECCC- Environment and Climate Change Canada (1 site), and JMA – Japan Meteorological Agency (3 sites). Data until 2019 are taken from obspack_co2_1_GLOBALVIEWplus_v6.1_2021-03-01, and JMA data are taken from WDCGG. Extension to GVplus_6.1 for 2020 is compiled from GML/NOAA data and WDCGG as appropriate.

Site_Name	Lat	Long	Alt(m)	Operating Institute
co2_alt_surface-flask_1_representative	82.5	-62.5	190.0	GML/NOAA
co2_asc_surface-flask_1_representative	-8.0	-14.4	85.0	GML/NOAA
co2_ask_surface-flask_1_representative	23.3	5.6	2710.0	GML/NOAA
co2_azr_surface-flask_1_representative	38.8	-27.4	19.0	GML/NOAA

co2_bmw_surface-flask_1_representative	32.3	-64.9	30.0	GML/NOAA
co2_brw_surface-flask_1_representative	71.3	-156.6	11.0	GML/NOAA
co2_cba_surface-flask_1_representative	55.2	-162.7	21.3	GML/NOAA
co2_cgo_surface-flask_1_representative	-40.7	144.7	94.0	GML/NOAA
co2_chr_surface-flask_1_representative	1.7	-157.2	0.0	GML/NOAA
co2_crz_surface-flask_1_representative	-46.4	51.8	197.0	GML/NOAA
co2_eic_surface-flask_1_representative	-27.2	-109.4	47.0	GML/NOAA
co2_gmi_surface-flask_1_representative	13.4	144.7	0.0	GML/NOAA
co2_hba_surface-flask_1_representative	-75.6	-26.2	30.0	GML/NOAA
co2_hun_surface-flask_1_representative	47.0	16.7	248.0	GML/NOAA
co2_ice_surface-flask_1_representative	63.4	-20.3	118.0	GML/NOAA
co2_izo_surface-flask_1_representative	28.3	-16.5	2372.9	GML/NOAA
co2_key_surface-flask_1_representative	25.7	-80.2	1.0	GML/NOAA
co2_kum_surface-flask_1_representative	19.5	-154.8	3.0	GML/NOAA
co2_mhd_surface-flask_1_representative	53.3	-9.9	5.0	GML/NOAA
co2_mid_surface-flask_1_representative	28.2	-177.4	11.0	GML/NOAA
co2_mlo_surface-flask_1_representative	19.5	-155.6	3397.0	GML/NOAA
co2_nmb_surface-flask_1_representative	-23.6	15.0	456.0	GML/NOAA
co2_nwr_surface-flask_1_representative	40.1	-105.6	3523.0	GML/NOAA
co2_psa_surface-flask_1_representative	-64.9	-64.0	10.0	GML/NOAA
co2_rpb_surface-flask_1_representative	13.2	-59.4	15.0	GML/NOAA
co2_sey_surface-flask_1_representative	-4.7	55.5	2.0	GML/NOAA
co2_shm_surface-flask_1_representative	52.7	174.1	23.0	GML/NOAA
co2_smo_surface-flask_1_representative	-14.2	-170.6	42.0	GML/NOAA
co2_spo_surface-flask_1_representative	-89.0	-24.8	2810.0	GML/NOAA
co2_sum_surface-flask_1_representative	72.6	-38.4	3209.5	GML/NOAA
co2_syo_surface-flask_1_representative	-69.0	39.6	14.0	GML/NOAA

co2_tap_surface-flask_1_representative	36.7	126.1	16.0	GML/NOAA
co2_ush_surface-flask_1_representative	-54.8	-68.3	12.0	GML/NOAA
co2_uta_surface-flask_1_representative	39.9	-113.7	1327.0	GML/NOAA
co2_uum_surface-flask_1_representative	44.5	111.1	1007.0	GML/NOAA
co2_wis_surface-flask_1_representative	30.0	35.1	151.0	GML/NOAA
co2_wlg_surface-flask_1_representative	36.3	100.9	3810.0	GML/NOAA
co2_zep_surface-flask_1_representative	78.9	11.9	474.0	GML/NOAA
co2_cfa_surface-flask_2_representative	-19.3	147.1	2.0	CSIRO
co2_mqa_surface-flask_2_representative	-54.5	159.0	6.0	CSIRO
co2_cya_surface-flask_2_representative	-66.3	110.5	47.0	CSIRO
co2_maa_surface-flask_2_representative	-67.6	62.9	32.0	CSIRO
co2_ams_surface-insitu_11_representative	-37.8	77.5	55.0	LSCE/IPSL
co2_bhd_surface-flask_426_representative	-41.4	174.9	85.0	SIO-CO2
co2_rk1_surface-flask_426_representative	-29.2	-177.9	2.0	SIO-CO2
co2_cpt_surface-insitu_36_marine	-34.4	18.5	230.0	SAWS
co2_fsd_surface-insitu_6_allvalid	49.9	-81.6	210.0	ECCC
co2_mnm_surface-insitu_19_representative	24.3	154.0	8.0	JMA
co2_ryo_surface-insitu_19_representative	39.0	141.8	260.0	JMA
co2_yon_surface-insitu_19_representative	24.5	123.0	30.0	JMA

Table S2. The prior and predicted CO2 fluxes (in PgC yr^{-1}) for 15 land and 11 ocean regions for 2001 - 2020. The predicted fluxes are shown for ensemble mean of "gc3t", "gvjf" and all cases ("ensm"). The gc3t are based on the CASA fluxes for land and Takahashi fluxes for ocean. The gvjf prior is based on VISIT+GFED fluxes for land and JMA fluxes for ocean. The "ensm" is the ensemble mean of both gc3t and gvjf cases. The spread denotes the 1-sigma deviation from the mean CO2 flux of 8-8 ensemble inversion cases for gc3t and gvjf as well as 16 ensemble inversion cases for "ensm".

Land Regions	Prior (gc3t/gvjf)	Predicted gc3t, gvjf, **ensm** (mean ± spread)	Ocean Regions	Prior (gc3t/gvjf)	Predicted gc3t, gvjf, **ensm** (mean ± spread)
Boreal N. America	0.0/-0.49	-0.34 ±0.07 -0.42±0.11 **-0.38±0.10**	Northern Ocean	-0.28 / -0.28	-0.27±0.03 -0.01±0.10 **-0.14±0.15**
Temp. N. America	0.0/-0.33	-0.60±0.11 -0.59±0.16 **-0.59±0.14**	North Pacific	-0.51/-0.60	-0.59±0.01 -0.51±0.04 **-0.55±0.05**
Tropical America	0.0/-0.17	0.04±0.08 -0.01±0.04 **0.02±0.07**	South Pacific	-0.31/-0.54	-0.3±0.01 -0.48±0.01 **-0.39±0.09**
Central America	0.0/-0.33	-0.04±0.06 -0.24±0.03 **-0.14±0.11**	East Pacific	0.41 / 0.42	0.48±0.04 0.46±0.02 **0.47±0.03**
Temp. S. America	0.0/-0.36	0.04±0.06 -0.23±0.07 **-0.10±0.15**	West Pacific	0.06 / 0.06	0.06±0.0 0.07±0.01 **0.07±0.01**
Northern Africa	0.0/0.03	-0.11±0.02 -0.0±0.05 **-0.06±0.07**	North Atlantic	-0.21 / -0.27	-0.28±0.02 -0.27±0.01 **-0.27±0.02**
Central Africa	0.0/0.12	-0.18±0.07 0.1±0.05 **-0.04±0.15**	Tropical Atlantic	0.11 / 0.08	0.12±0.01 0.09±0.0 **0.11±0.02**
Southern Africa	0.0/0.15	-0.08±0.01 0.17±0.01 **0.05±0.12**	South Atlantic	-0.15 / -0.33	-0.17±0.01 -0.31±0.01 **-0.24±0.07**
Europe	0.0/-0.54	0.08±0.07 -0.09±0.08	Tropical Indian	0.12 / 0.12	0.07±0.02 0.1±0.02

		-0.0±0.11			**0.09±0.03**
North Asia	0.0/-0.76	-0.37±0.03 -0.33±0.05 **-0.35±0.05**	South Indian	-0.43 / 0.53	-0.43±0.01 -0.49±0.02 **-0.46±0.03**
West Asia	0.0/-0.11	-0.04±0.04 -0.09±0.01 **-0.06±0.04**	Southern Ocean	-0.23 / -0.24	-0.29±0.02 -0.18±0.02 **-0.23±0.06**
South Asia	0.0/-0.23	-0.10±0.10 -0.26±0.04 **-0.18±0.11**	**Global Total**		
East Asia	0.0/-0.55	-0.42±0.05 -0.57±0.04 **-0.49±0.09**	**Land**	0/-3.93	-2.42±0.10 -2.73±0.20 **-2.58±0.22**
Southeast Asia	0.0/-0.17	-0.25±0.08 0.0±0.05 **-0.13±0.15**	**Ocean**	-1.4/-2.11	-1.58±0.04 -1.51±0.07 **-1.54±0.13**
Oceania	0.0/-0.2	-0.06±0.07 -0.17±0.03 **-0.12±0.08**	**Land+Ocean**	-1.4/-6.06	-4.01±0.08 -4.26±0.07 **-4.14±0.14**

Table S3: *Correlation coefficient (r) between the mean CO2 flux (predicted/prior) anomaly and climate indices ENSO for 2001-2020 (columns 2-4). Correlation coefficients for the prior and predicted mean seasonal cycles are given in the two columns on the right.*

Regions	**r for interannual variability**			**r for seasonal cycle**	
	gc3t (predicted)	gvjf (predicted)	gvjf (prior)	prior gct3-gvjf	predicted gc3t-gvjf
Land Regions					
Boreal N. America	-0.05	0.07	0.1	0.77	0.9
Temp. N. America	-0.07	-0.26	-0.2	0.8	0.97
Tropical America	0.44	0.22	0.28	0.23	0.63
Central America	0.32	**0.47**	0.48	0.39	0.94
Temp. S. America	**0.54**	0.08	-0.04	0.88	0.74
Europe	0.19	0.23	0.09	0.83	0.92
Northern Africa	**0.46**	0.26	0.15	0.91	0.88
Central Africa	**0.51**	0.39	0.29	-0.19	0.04
Southern Africa	0.26	0.26	0.23	0.90	0.95
North Asia	-0.01	-0.11	-0.08	0.79	0.92
West Asia	0.19	0.16	0.06	0.83	0.91
South Asia	0.2	0.1	0.09	0.28	0.23
East Asia	0.03	-0.17	-0.21	0.28	0.83
Southeast Asia	0.29	**0.61**	**0.62**	0.19	0.15
Oceania	0.17	0.54	0.56	-0.48	-0.36
Ocean regions					
Northern Ocean	0.09	0.28	0.16	-0.16	0.46
North Pacific	0.1	0.02	-0.13	0.99	0.69
East Pacific	0.1	**-0.35**	-0.49	0.69	0.83

West Pacific	0.09	**-0.62**	**-0.7**	-0.33	0.69
South Pacific	-0.1	-0.24	-0.11	0.97	0.98
North Atlantic	-0.19	-0.14	-0.17	0.99	0.92
Tropical Atlantic	**0.39**	**0.38**	0.1	-0.10	0.63
South Atlantic	0.0	0.04	0.01	0.52	0.65
Tropical Indian	**0.36**	0.09	0.05	0.93	0.78
South Indian	**0.32**	0.25	0.07	0.94	0.95
Southern Ocean	0.23	0.11	-0.08	0.89	0.91

Table S4. Mean bias at different atmospheric layers for individual aircraft observations sites for their available period. Biases greater than ±2 ppm are marked in red, and those greater than ±1 ppm is marked in blue.

Site name	LT (0 -2 Km)		MT (3-5 Km)		UT (6-8 Km)		All (0 - 8 Km)	
	Mean Bias (ppm)	# of data points	Mean Bias (ppm)	# of data points	Mean Bias (ppm)	# of data points	Mean Bias (ppm)	# of data points
co2_aao_aircraft-pfp_1_allvalid	0.11	1442	0.48	784	nan	0	0.28	2810
co2_above_aircraft-insitu_1_allvalid	0.1	44443	1.31	27232	nan	0	0.77	95415
co2_above_aircraft-pfp_1_allvalid	-0.16	193	1.92	74	nan	0	0.75	344
co2_acg_aircraft-insitu_1_allvalid	-0.87	4251	1.32	1683	2.23	4310	0.9	14313
co2_acg_aircraft-pfp_1_allvalid	-0.22	675	1.03	264	0.91	296	0.43	1520
co2_act_aircraft-insitu_428_allvalid-b200	-0.47	198597	0.34	81425	-0.57	17218	-0.17	347177
co2_act_aircraft-insitu_428_allvalid-c130	-0.1	122769	0.34	87700	-0.09	40766	0.06	347919
co2_act_aircraft-pfp_1_allvalid-b200	-0.95	1987	0.39	563	-0.3	123	-0.49	3022
co2_act_aircraft-pfp_1_allvalid-c130	-0.14	1451	0.58	614	-0.04	240	0.1	2897
co2_aia_aircraft-flask_2_represe	-0.14	160	0.01	82	0.1	51	-0.05	353

ntative								
co2_alf_aircraft-pfp_26_representative	-0.06	333	0.01	245	nan	0	-0.09	684
co2_aoa_aircraft-flask_19_allvalid	-0.04	206	-0.18	237	-0.03	1161	-0.04	2500
co2_arcpac2008_aircraft-insitu_114_allvalid	0.01	7489	-1.13	6146	-0.49	3493	-0.66	22586
co2_arctas_aircraft-insitu_428_allvalid-dc8	-1.25	17529	0.07	10376	0.42	9382	-0.38	46730
co2_bgi_aircraft-pfp_1_allvalid	-0.99	71	0.23	93	-0.08	89	-0.13	334
co2_bne_aircraft-pfp_1_allvalid	-0.46	259	-0.08	248	-0.45	218	-0.28	972
co2_brz_aircraft-insitu_20_allvalid	-0.31	77277	1.82	2778	nan	0	0.11	100259
co2_calnex2010_aircraft-insitu_114_allvalid	-3.66	29604	-0.19	4234	0	40	-2.7	39366
co2_car_aircraft-pfp_1_allvalid	-1.33	138	0	2548	-0.01	1964	-0.07	6698
co2_cma_aircraft-pfp_1_allvalid	-1.09	803	0.41	541	-0.11	546	-0.28	2610
co2_cob2003b_aircraft-insitu_59_allvalid	0.45	5228	0.95	3973	0.38	4122	0.66	16692
co2_cob2004_a	-0.6	18052	1.21	10328	1.75	11583	0.82	50688

ircraft-insitu_59_allvalid								
co2_cob_aircraft-flask_1_allvalid	-0.78	61	-1.03	18	-0.56	1	-0.54	108
co2_cob_aircraft-insitu_59_allvalid	2.53	17434	1.09	16319	0.95	8037	1.52	55783
co2_cob_aircraft-pfp_1_allvalid	1.39	68	0.27	73	0.69	30	0.7	227
co2_con_aircraft-flask_42_allvalid	-0.22	9	-0.34	14	-0.32	26	-0.31	65
co2_con_aircraft-insitu_42_allvalid	-1.23	504283	-0.39	670363	-0.25	631220	-0.55	2449936
co2_crv_aircraft-pfp_1_allvalid	-2.59	1601	0.95	107	nan	0	-1.68	2103
co2_dc3_aircraft-insitu_428_allvalid-dc8	0.6	6800	-0.72	5511	-1.21	3656	-0.36	21178
co2_dc3_aircraft-insitu_428_allvalid-falcon	1.64	1066	-2.33	3711	-2.13	4074	-1.7	12459
co2_discover-aq_aircraft-insitu_428_allvalid-c130-co	-9.47	5968	-0.44	8304	-1.19	301	-3.57	21114
co2_discover-aq_aircraft-insitu_428_allvalid-p3b-ca	-5.82	18973	-0.46	640	nan	0	-4.2	26822
co2_discover-aq_aircraft-	-7.43	8194	-0.81	8840	-0.55	49	-3.5	30057

insitu_428_allvalid-p3b-co								
co2_discover-aq_aircraft-insitu_428_allvalid-p3b-tx	-4.42	14239	0.43	6416	0.5	932	-2.36	25077
co2_dnd_aircraft-pfp_1_allvalid	-0.49	547	0.18	487	0.12	438	-0.02	2075
co2_eco_aircraft-insitu_1_allvalid	-2.19	26197	-0.31	1463	nan	0	-1.95	30468
co2_esp_aircraft-pfp_1_allvalid	-0.4	1772	0.37	1494	nan	0	0.08	4563
co2_etl_aircraft-pfp_1_allvalid	-0.47	1082	0.56	638	0.59	276	0.12	3184
co2_ftl_aircraft-pfp_1_allvalid	-0.18	12	0.39	51	nan	0	0.17	90
co2_fwi_aircraft-pfp_1_allvalid	-0.39	79	0.29	102	0.15	95	0.17	361
co2_gsfc_aircraft-insitu_430_allvalid	0.38	5903	0.8	11968	0.81	16066	0.77	43427
co2_haa_aircraft-pfp_1_allvalid	0.03	260	-0.13	543	0.04	370	-0.07	1627
co2_hfm_aircraft-pfp_1_allvalid	-1.08	451	0.37	392	0.15	361	-0.14	1630
co2_hil_aircraft-pfp_1_allvalid	-0.48	593	-0.2	727	-0.36	672	-0.31	2622
co2_hip_aircraft-insitu_59_allvalid	-0.14	21818	0.42	19025	0.31	18172	0.21	77048
co2_iagos-caribic_aircraft-flask_457_allva	1.97	2	-0.19	29	-0.16	29	-0.11	74

lid								
co2_iagos-caribic_aircraft-insitu_457_allvalid	-1.18	993	0.58	1768	0.65	6053	0.45	11322
co2_intex-b_aircraft-insitu_428_allvalid-dc8	-0.45	1692	-0.27	1327	-0.48	1118	-0.37	5447
co2_intex-na_aircraft-insitu_428_allvalid-dc8	2.56	14469	1.61	7889	1.55	7626	2.08	36495
co2_inx_aircraft-pfp_1_allvalid	-2.56	238	0.11	12	nan	0	-2.23	273
co2_korus-aq_aircraft-insitu_428_allvalid-dc8	-3.84	34197	-0.08	5307	-0.56	9006	-2.49	55612
co2_lef_aircraft-pfp_1_allvalid	-0.29	1884	0.25	1115	nan	0	-0.03	3976
co2_mci_aircraft-pfp_1_allvalid	-1.29	65	-0.5	10	nan	0	-1.14	92
co2_mrc_aircraft-pfp_1_allvalid	0.15	58	-0.32	1	nan	0	0.13	65
co2_nha_aircraft-pfp_1_allvalid	-0.9	1373	0.45	789	0.06	536	-0.21	3633
co2_oil_aircraft-pfp_1_allvalid	-0.05	87	0.51	113	0.11	106	0.31	399
co2_orc_aircraft-insitu_3_allvalid-merge10	-0.14	8027	-0.16	3635	-0.04	3911	-0.12	19414
co2_pfa_aircraft-pfp_1_allvalid	0.08	1152	0.41	1327	0.51	781	0.28	4522
co2_rba-b_aircraft-	-0.66	334	-0.47	231	nan	0	-0.65	674

pfp_26_representative								
co2_rta_aircraft-pfp_1_allvalid	0.18	437	0.03	792	0.12	332	0.06	2235
co2_sam_aircraft-pfp_1_allvalid	-0.68	35	-1.31	29	-0.59	23	-1.08	118
co2_san_aircraft-pfp_1_allvalid	0.3	11	-0.26	90	nan	0	-0.3	154
co2_san_aircraft-pfp_26_representative	-0.82	1309	-0.31	719	nan	0	-0.66	2458
co2_sca_aircraft-pfp_1_allvalid	-0.84	525	-0.02	811	-0.32	746	-0.24	2892
co2_seac4rs_aircraft-insitu_428_allvalid-ER2	0.82	4	1.1	233	0.54	210	0.81	590
co2_seac4rs_aircraft-insitu_428_allvalid-dc8	1.03	18802	0.09	6688	0.69	6991	0.75	39914
co2_senex2013_aircraft-insitu_114_allvalid	0.9	30012	1.04	4440	1.1	467	0.88	39610
co2_sgp_aircraft-pfp_1_allvalid	-0.22	2374	-0.25	1623	1.08	9	-0.23	5513
co2_songnex2015_aircraft-insitu_114_allvalid	0.04	20404	-0.11	5418	-0.78	4398	-0.1	42549
co2_start08_aircraft-insitu_59_allvalid	-0.85	1421	-0.46	2548	-0.54	1985	-0.57	8107
co2_tab_aircraft-	-1.98	228	-0.48	163	nan	0	-1.33	463

pfp_26_representative								
co2_texaqs2006_aircraft-insitu_114_allvalid	-4.48	28586	0.5	2046	nan	0	-3.87	32653
co2_tgc_aircraft-pfp_1_allvalid	-0.65	382	-0.34	694	-0.36	594	-0.37	2337
co2_thd_aircraft-pfp_1_allvalid	-1.06	598	0.32	589	-0.05	535	-0.15	2329
co2_tom_aircraft-insitu_1_allvalid	0.02	25586	0.13	15139	0.17	17915	0.1	74184
co2_trace-p_aircraft-insitu_428_allvalid-dc8	-0.07	11133	-0.18	7003	-0.34	6097	-0.2	30887
co2_trace-p_aircraft-insitu_428_allvalid-p3b	0.32	16956	-0.15	13902	0.1	6935	0.04	50121
co2_ulb_aircraft-pfp_1_allvalid	0.36	169	0.17	223	nan	0	0.28	546
co2_wbi_aircraft-pfp_1_allvalid	-0.4	532	0.01	653	-0.36	617	-0.22	2366

Testing the effect of Cyc-G vs Cyc-Met

This quasi-IAV meteorology approach has been done first in Patra et al. (JMSJ, 2016) followed by Chandra et al., 2021.

In our inversion system, monthly-mean regional a posteriori fluxes (S) are based on the observation data (D_{obs}) and model simulation (D_{ACTM}) of a priori fluxes (S_0) (Eq. 2). This equation shows that the a priori model simulation D_{ACTM} is the most important term for the correction (increase or decrease) of the a priori fluxes. Green's function determines the magnitude of flux corrections. Noting the importance of the (D-M) term compared to G, while the latter is 84 (inversion region) x 12 (months per year) x 4 (pulse duration) times more computationally expensive, we have decided to put more focus on D_{ACTM}, e.g., testing various emission combinations, transport sensitivity in this study. The figure below shows an example of the "CO2" inversion case for IAV meteorology and quasi-IAV meteorology (2009 G-matrix). This plot clearly shows that the flux anomalies can be consistently estimated by the inverse modelling by our quasi-IAV approach.

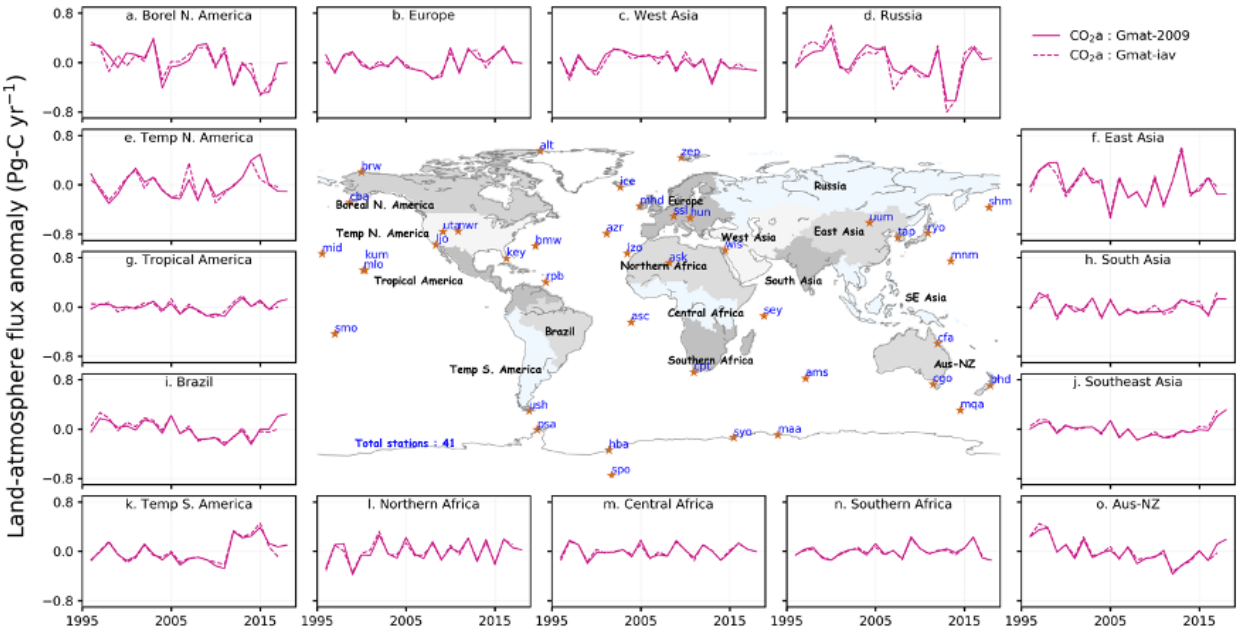

Figure S1: Regional CO_2 fluxes anomalies, similar to Fig. 6, for showing the effect of inter-annually varying G-matrix (Gmat-iav) vs annually repeating G-matrix corresponding to the year 2009 (Gmat-2009). This checking was conducted using the inversion results submitted to GCP-2018 budget (Le Quere et al., ESSD, 2018), which clearly suggested the role of interannully varying winds did not have significant roles in estimation of regional fluxes and the flux variability while it is well-known that the forward simulation of a priori fluxes must use interannually varying winds and temperature.

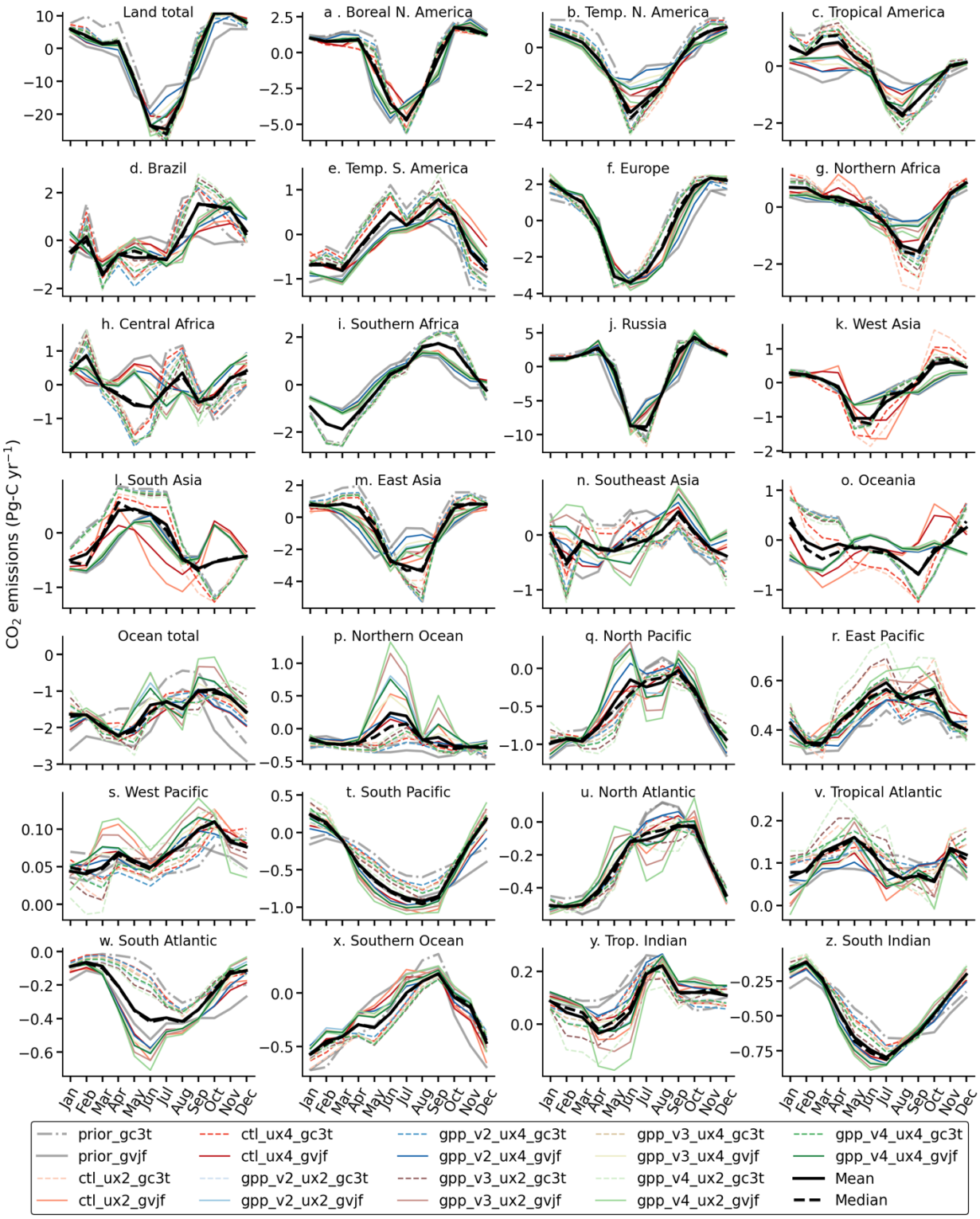

Figure S2. Seasonal variations in monthly-mean CO fluxes at regional scales over 15 land (upper 4 rows) and 11 ocean (lower 3 rows) regions, along with global land and ocean totals. Note that all panels use different y-scale.

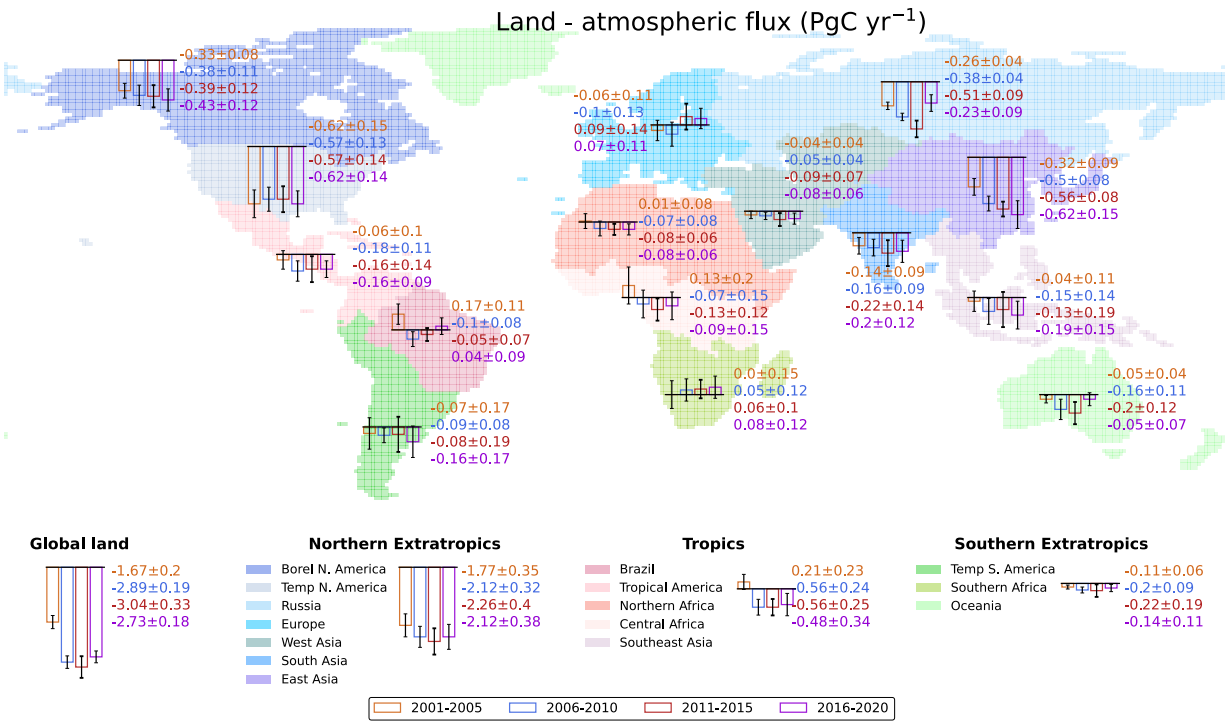

Fig S3. Mean CO_2 fluxes and spread ($\pm 1\sigma$) among 16 inversion cases over global, three aggregated latitudinal bands and 15 aggregated land regions. The bars in the down-facing directions represent carbon sinks, whereas the bars in the upward-facing directions represent carbon source.

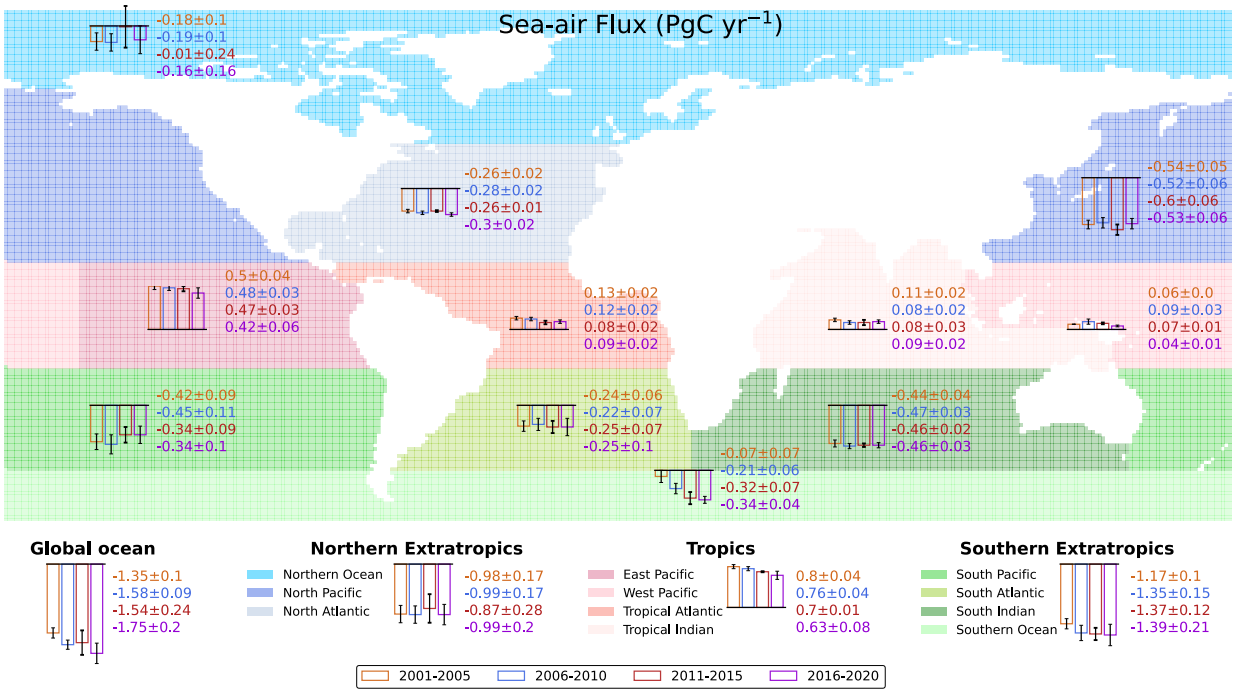

Fig S4. Mean CO_2 fluxes and spread among 16 inversion cases ($\pm 1\sigma$) over global, three aggregated latitudinal bands and 11 aggregated ocean regions. The bars in the down-facing directions represent carbon sinks, whereas the bars in the upward-facing directions represent carbon source.

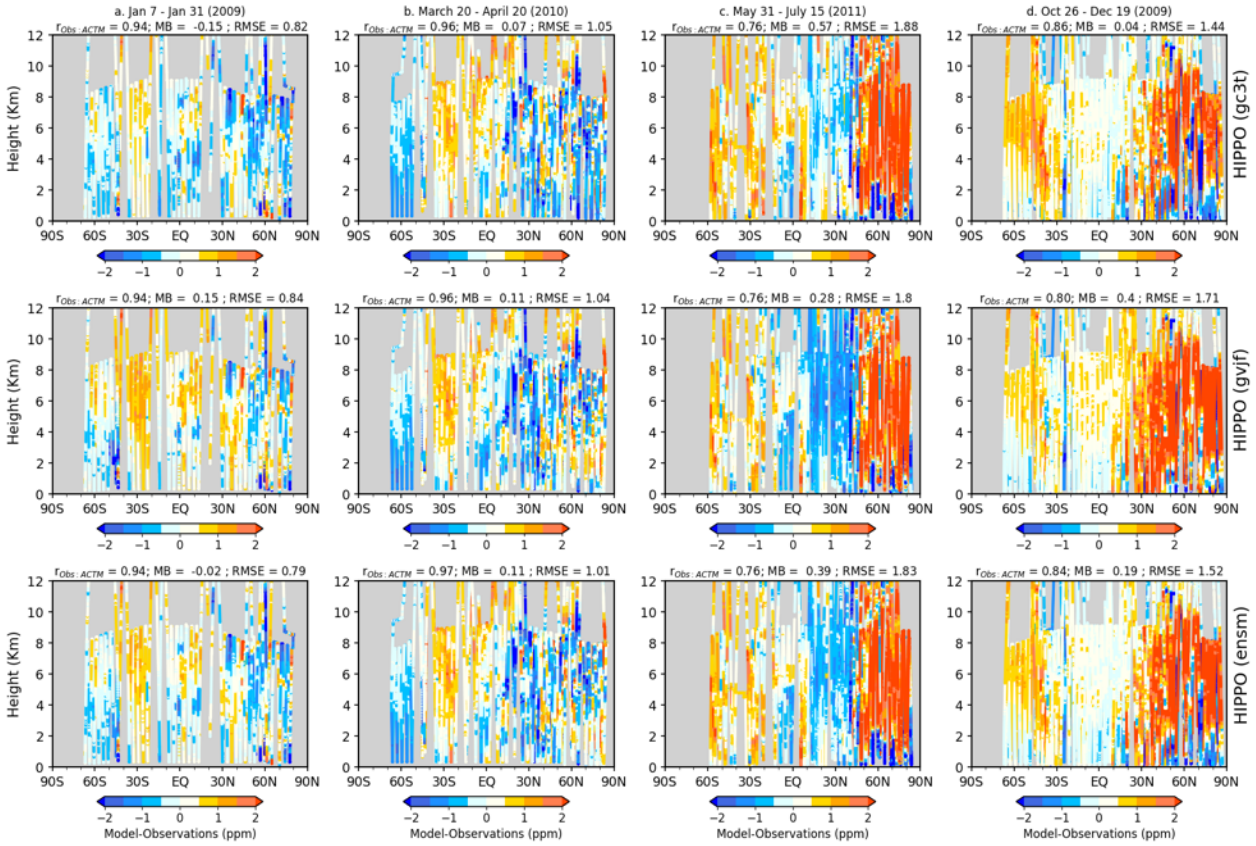

Figure S5: Mismatch between simulated and measured CO2 during HIPPO aircraft campaigns. The observed and modelled data are binned and averaged at intervals of 2.5^{o} latitude and 500-meter altitude. The grey area shows no flights at those altitudes and altitudes. Modelled mole fractions were simulated from the three posterior flux cases. The upper, middle, and the bottom row show simulations for "gc3t", "gvjf", and "ensm" cases, respectively. The correlation coefficients (r), mean bias (MB), and root-mean-square error between observations and simulations are also shown in the title.

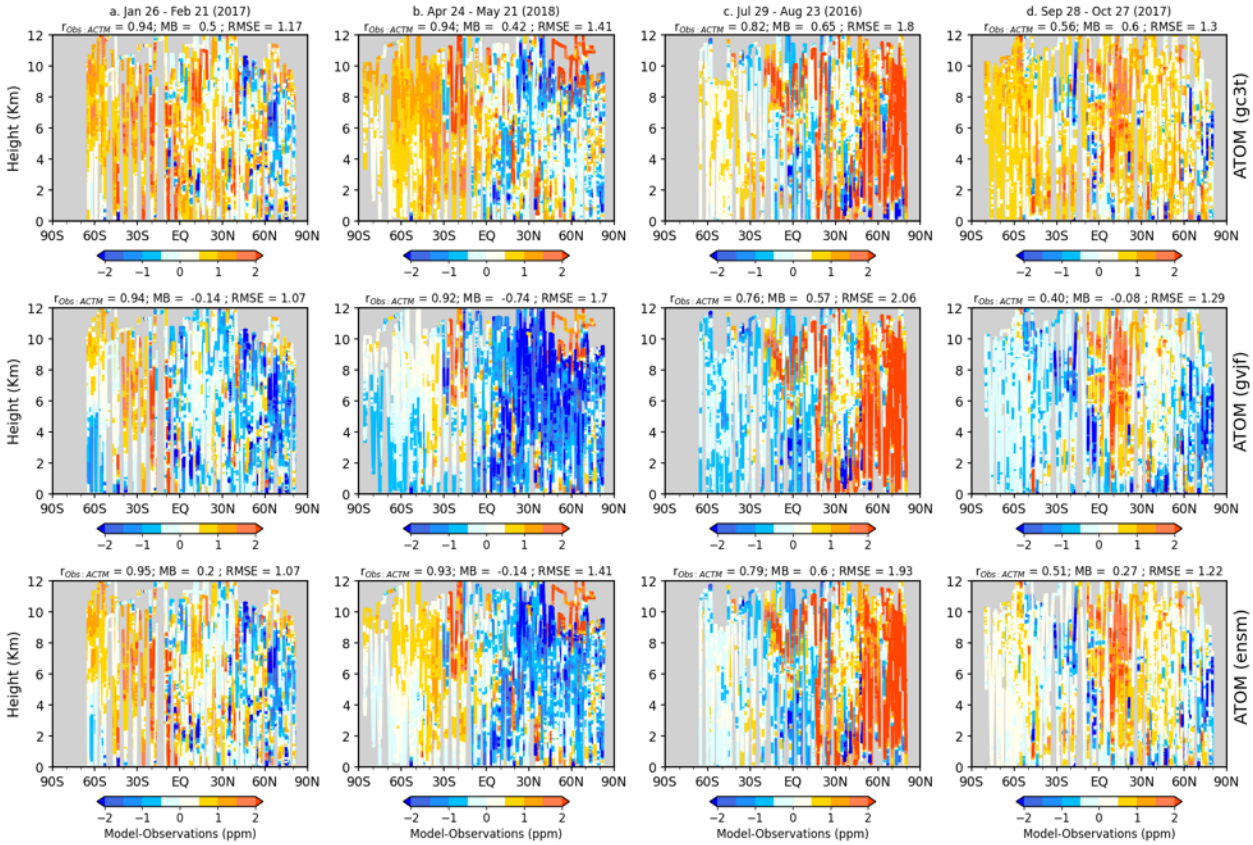

Figure S6: Same as S2, but for ATOM aircraft campaigns.

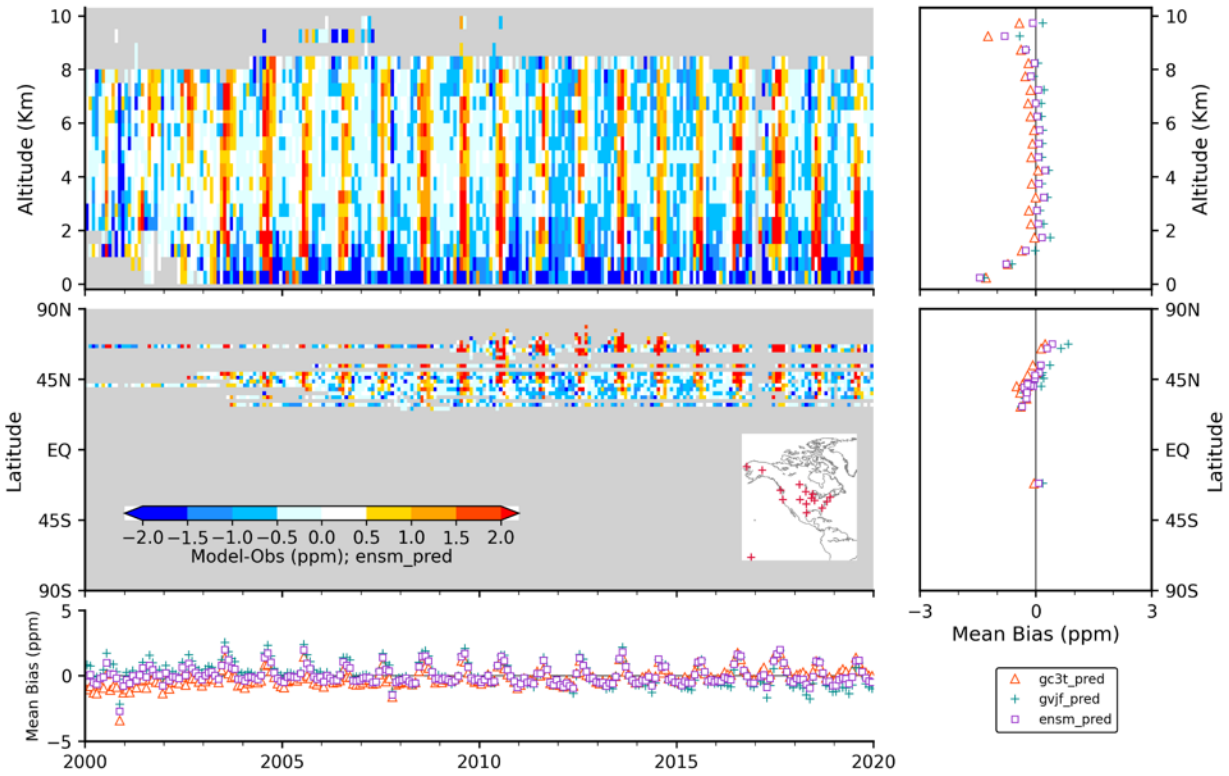

Figure S7. Validation of simulated CO_2 mixing ratios using regular NOAA aircraft profiles over 16 sites (see the location in the middle panel's inset map). The top panel shows bias (model minus observations) as a function of altitude, and the middle shows the mean bias in the free troposphere (defined between 2 and 8 Km) as a function of latitude. The bottom panel shows the monthly mean bias in the free troposphere over all the latitudes. The contour plots are shown for the "ensm" prescribed flux case, while other plots are shown for all three prescribed emission cases.

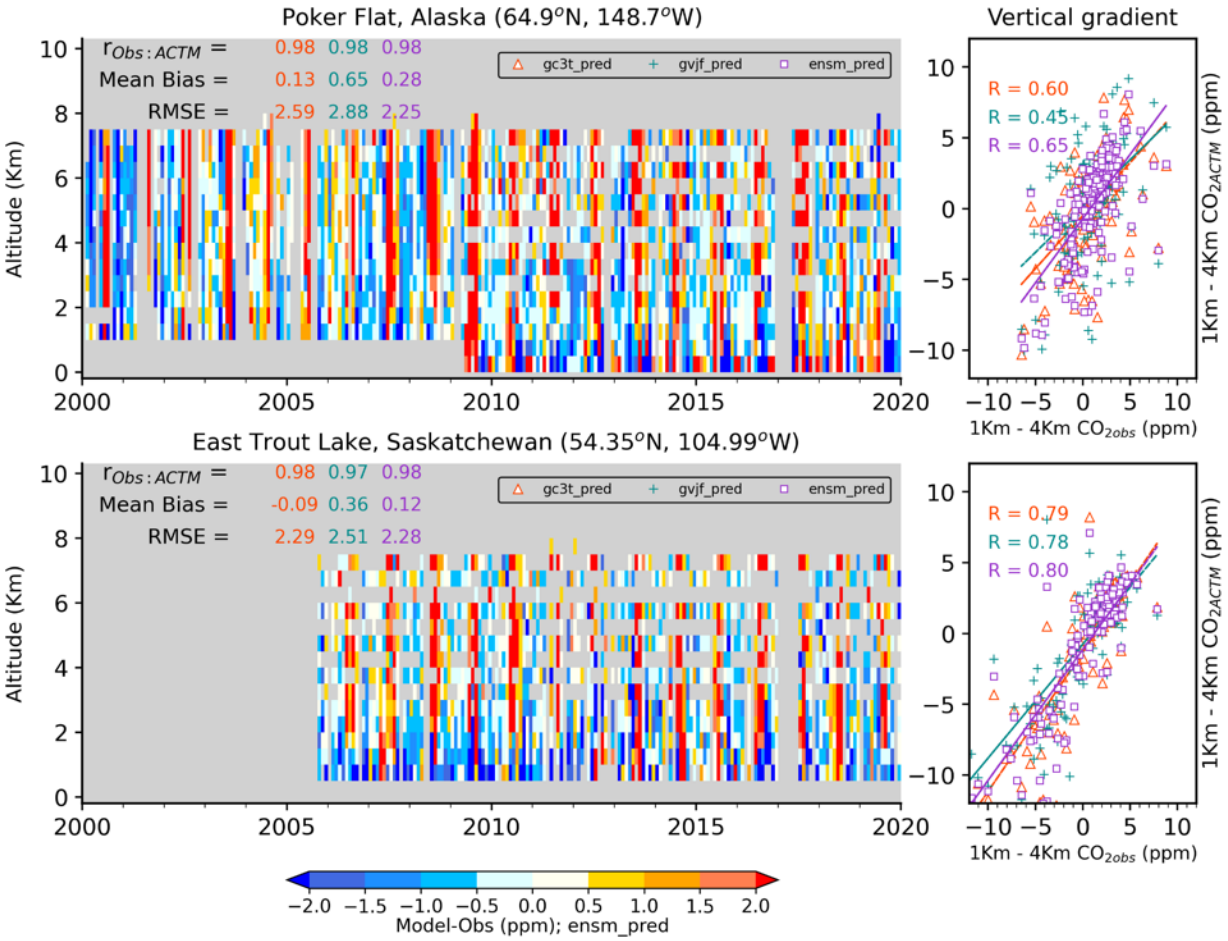

Figure S8. Validation of simulated CO_2 mixing ratios using regular NOAA aircraft profiles over two sites located in boreal North America (see also Figure xx for the location of profiles). The left panel shows the bias (model minus observations) as a function of altitude, and the right panel shows the scatter plot between the observed and modelled vertical gradient using three prescribed emissions.

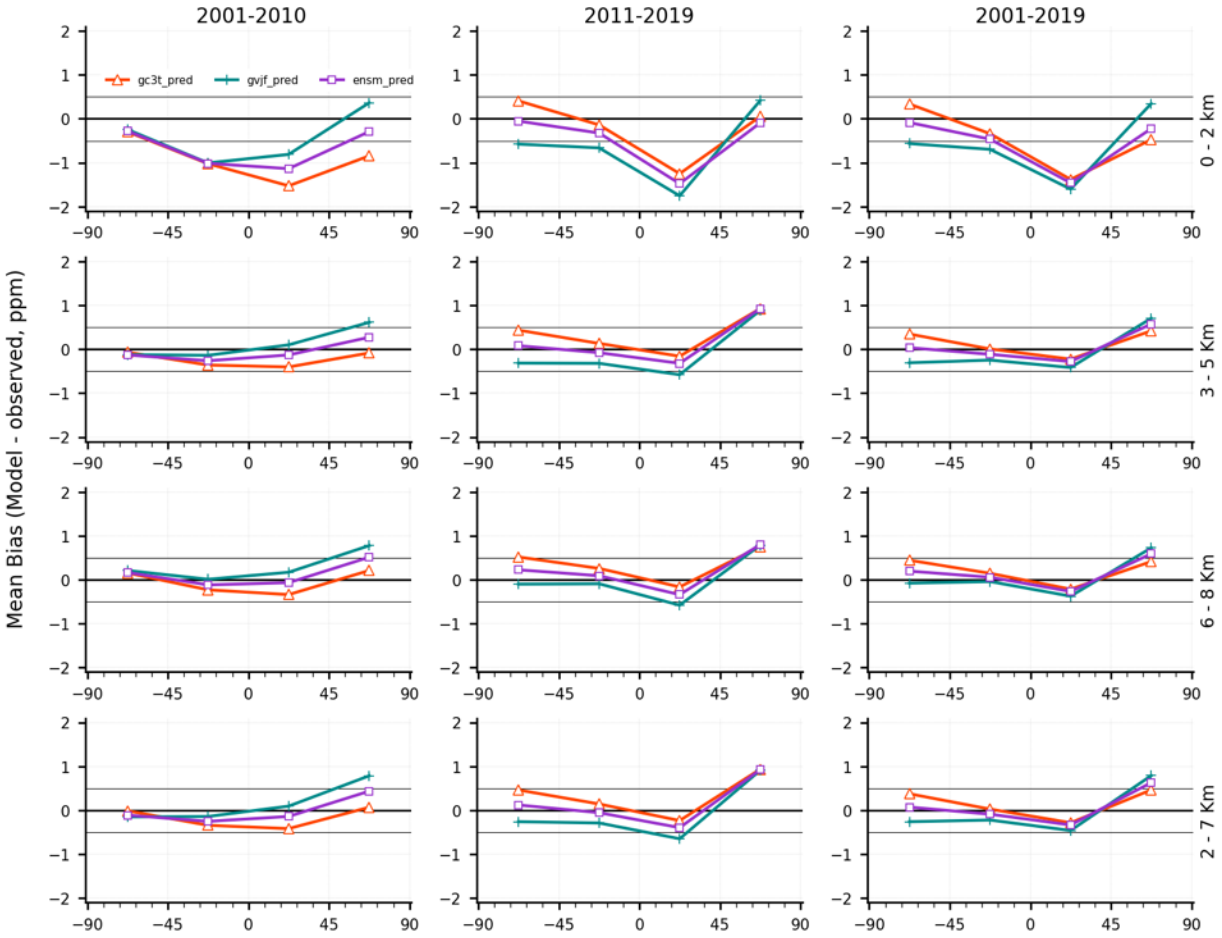

Figure S9. Evaluation of the atmospheric inversion products. The mean of the model minus observations is shown for four latitude bands at four altitude ranges in three periods: **(a)** 2001–2010, **(b)** 2011–2020, **(c)** 2001–2020. The simulations from three inversion cases are compared to independent CO_2 measurements made onboard aircraft over many places of the world between 2 and 8 km above sea level. Aircraft measurements archived in the Cooperative Global Atmospheric Data Integration Project (CGADIP, 2020) from sites, campaigns, or programs that cover at least 9 months between 2001 and 2020, and that have not been assimilated have been used to compute the biases of the differences in four 45˚ latitude bins. Land and ocean data are used without distinction.

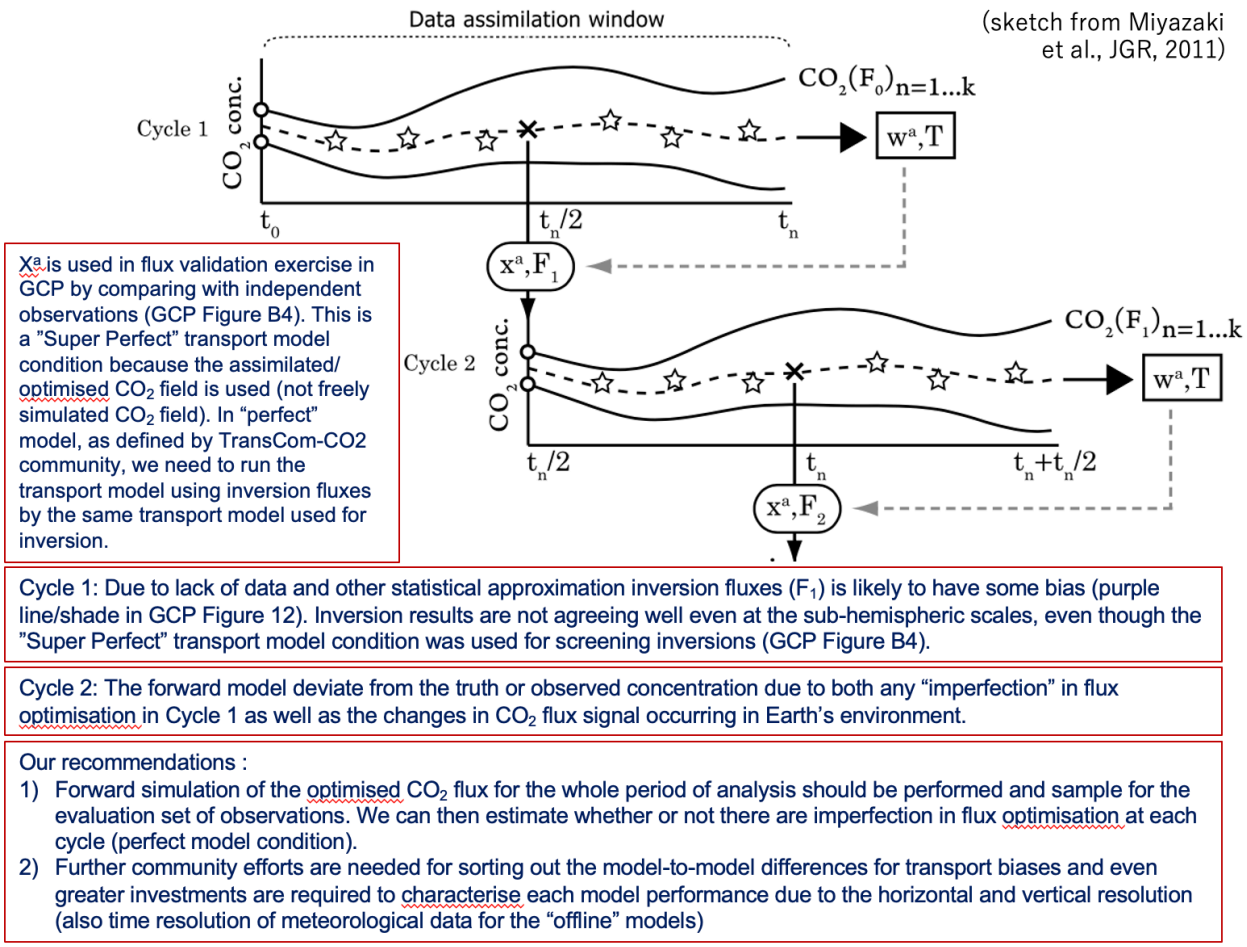

Figure S10. Schematic diagram showing the issue of "Super perfect" and "Perfect" model conditions in inverse modelling, and our 2-step recommendations for evaluation of future model intercomparison.